We are IntechOpen, the world's leading publisher of Open Access books Built by scientists, for scientists

6,900
Open access books available

185,000
International authors and editors

200M
Downloads

Our authors are among the

154
Countries delivered to

TOP 1%
most cited scientists

12.2%
Contributors from top 500 universities



WEB OF SCIENCE™

Selection of our books indexed in the Book Citation Index in Web of Science™ Core Collection (BKCI)

Interested in publishing with us?
Contact book.department@intechopen.com

Numbers displayed above are based on latest data collected.
For more information visit www.intechopen.com



Chapter

Micro-/Nano-Structuring in Stainless Steels by Metal Forming and Materials Processing

Tatsuhiko Aizawa, Tomomi Shiratori and Takafumi Komatsu

Abstract

Austenitic stainless steel type AISI304 sheets and plates as well as fine-grained type AISI316 (FGSS316) substrates and wires were employed as a work material in the intense rolling, the piercing and the plasma nitriding. AISI304 sheet after intense rolling had textured microstructure in the rolling direction. Crystallographic state changed itself to have distorted polycrystalline state along the shearing plane by piercing, with the strain induced phase transformation. FGSS316 substrates were plasma nitrided at 623 K for 14.4 ks to have two-phase fine nanostructure with the average grain size of 100 nm as a surface layer with the thickness of 30 μm. FGSS316 wires were also plasma nitrided at the same conditions to form the nitrided surface down to the depth of 30 μm. This nitrided wire was further uniaxially loaded in tensile to attain more homogeneously nitrided surface nano-structure and to form the austenitic and martensitic fiber structure aligned in the tensile direction. Each crystallographic structure intrinsic to metals and metallic alloys was tailored to have preferable micro–/nano-structured cells by metal forming and nitrogen supersaturation. The crystallographic change by metal forming in a priori and posterior to nitriding was discussed to find out a new way for materials design.

Keywords: micro-/nano-texturing, stainless steels, rolling, piercing, plasma nitriding, a priori metal forming to nitriding, posterior nitriding to metal forming

1. Introduction

Most of metals and metallic alloys have crystalline structure, intrinsic to each material property. This crystalline structure is classified by several items; e.g., single and poly-crystals, grain size, grain boundary characteristics, crystallographic orientation, and so forth [1]. These items are controllable by mechanical and chemical interaction with internally and externally straining [2]. For examples, a single crystal changes itself to polycrystalline state by introduction of dislocations with sufficiently high density [3]. The original grains are much refined by intense rolling [4] and by high shear straining [5]. The initial grain boundaries are also tunable by shuffling process through their interaction with dislocations [6]. That is, the crystalline structure is tailored by metal forming and materials processing to have preferable grain size, crystallographic orientations, and grain boundaries [7–9].

IntechOpen

Let us consider how to control the crystallographic structure of metals and metallic alloys by the technology of plasticity in metal forming and surface treatment. **Figure 1** depicts three case studies on the crystallographic structure change by rolling, shearing, and nitrogen supersaturation. Even when the initial grains are equiaxial, some of them are forced to partially align along the rolling direction. The skew distortion by intense rolling drives to shear the grains with spin-rotation as shown in **Figure 1a**. In case of embossing and piercing the sheet metals, the grains are distorted to plastically flow along the shearing plane with grain size refinement as depicted in **Figure 1b**. In the low temperature plasma nitriding, the plastic straining is induced by the nitrogen supersaturation into metallic lattices to form the slip-line system as shown in **Figure 1c**. Without externally applied stresses, the slip-line network is formed from the surface to the depth together with the nitrogen interstitial diffusion. In particular, the low temperature plasma nitriding process [10–15] works as a powerful means to demonstrate that austenitic and martensitic stainless steel substrates are hardened and modified to have two-phase structure with the average grain size of 0.1 μm. These previous studies proved that grain size as well as crystallographic structure should be significantly controlled by the materials processing other than the shearing process in metal forming.

In the present chapter, the crystallographic structure evolution of stainless steels during the rolling, the piercing, and the plasma nitriding at 623 K for 14.4 ks is first described to deduce the mechanism of microstructure evolution during metal forming and materials processing. Next, the uniaxial loading test of plasma nitrided work at 623 K is performed to investigate the possibility of further microstructure evolution during posterior metal forming. Through these experiments, the effect of the interstitial element concentration as well as the plastic straining on the crystallographic evolution is discussed to search for the materials science model to describe the interaction between the interstitial mobility and the plastic straining. In the following, EBSD (Electron Back Scattering Diffraction) is employed to make crystallographic analyses. This technique is based on the automatic analysis of the Kikuchi pattern by the excitation of the electron beam on the surface of the sample in SEM (Scanning Electron Microscope) [16]. Among several analytical tools in EBSD, the crystallographic orientation for each grain is described by IPF (Inverse Pole Figure) and the strain induced phase transformation is also analyzed by phase mapping. In addition, the equivalent plastic strain distribution is estimated by KAM (Kernel Angle Misorientation) mapping.

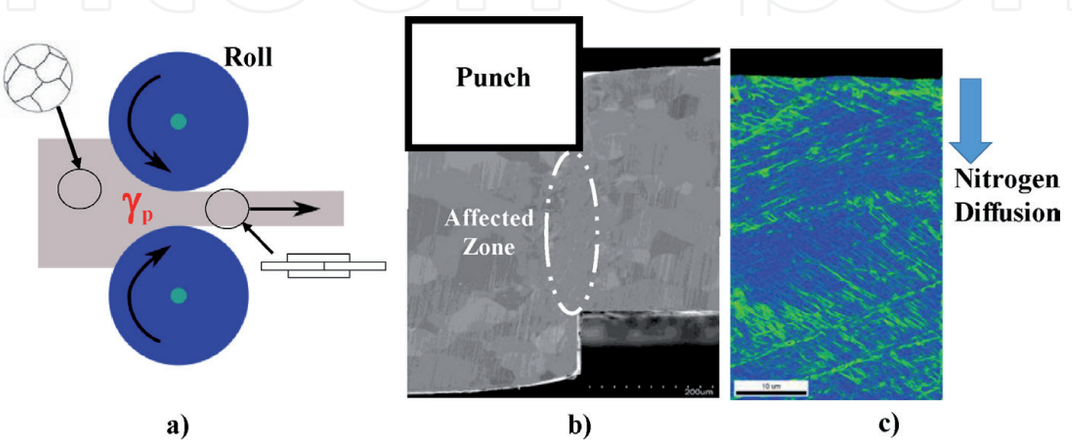


Figure 1.
Three types of crystallographic evolution during metal forming and plasma nitriding. (a) Intense rolling, (b) embossing and piercing, and (c) low temperature plasma nitriding.

2. Texture formation by intense rolling

Intense rolling with heat treatment has been utilized to fabricate the fine-grained stainless steel plates and sheets [4, 7, 17]. In the following, AISI304 sheet was employed as a work to reduce its thickness from 10 mm down to 1 mm by intense rolling. EBSD analysis was used to describe the crystallographic change in the rolled AISI304 sheet.

2.1 Rolling procedure

A typical rolling system was illustrated in **Figure 2a**. AISI304 sheet with the initial thickness of 10 mm was compressed and sheared between two work rolls in a single reduction. Since the reduction of thickness was 10% in this single rolling, nine steps were utilized to reduce the thickness down to 1 mm through this intense rolling. **Figure 2b** shows the rolled sheet by 90% reduction in thickness. This rolling is effective to reduce the average grain size of stainless steel works for embossing and piercing to be discussed in later.

2.2 Microstructure evolution by intense rolling

The original AISI304 sheet was characterized by three high intensity peaks in XRD analysis. As depicted in **Figure 3**, three peaks were detected in correspondence to γ (111), γ (200), and γ (220) planes in the austenitic phase. This microstructure changes to nearly full-martensitic phase; as also depicted in **Figure 3**, three martensitic peaks were detected as α' (211), α' (200), and α' (110) besides for γ (220) and γ (111). This proves that original austenitic grains massively transform to martensitic ones in AISI304 sheets during the intense rolling. These martensitic grains can be inversely transformed back to austenite by heat treatment. This technique is useful to reduce the average grain sizes to be stated later.

2.3 Controlled crystallographic structure by intense rolling

In addition to the strain-induced phase transformation in **Figure 3**, the intense rolling has much influence on the crystallographic structure in AISI304. **Figure 4** depicts the inverse pole figure mapping, the KAM distribution, and the phase mapping on the cross-section of rolled AISI304 sheet, analyzed by EBSD. As stated before, the average grain size is reduced down to 1 μm in most of AISI304, since the plastic strains are applied to these regions as shown in **Figure 4a** and **b**. Low plastic strained regions in **Figure 4b** corresponds to assembly of larger grains laterally aligned in the rolling direction. Through comparison between **Figure 4b** and **c**, these

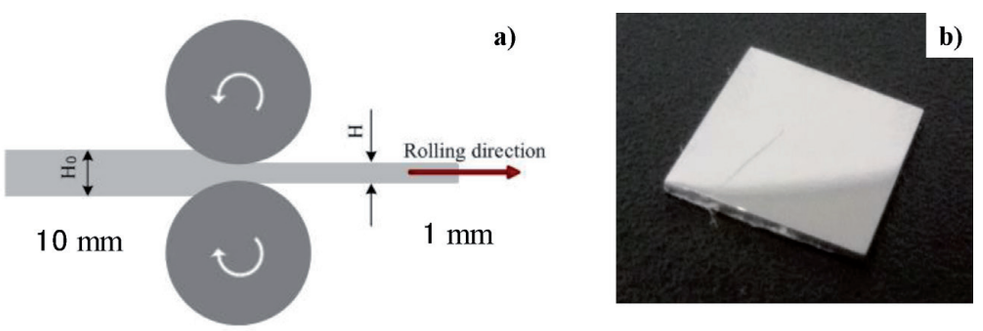


Figure 2.
Intense rolling process with high reduction in thickness. (a) Illustration on the rolling process in multi-steps for reduction of thickness by 90% and (b) rolled AISI304 sheet.

textures are classified into two zones. One is thin and long full-martensitic textures. The shorter and dotted textures are corresponding to the retained austenitic textures.

These textured crystallographic structures are further controlled by the low temperature plasma nitriding as well as the heat treatment to be discussed in later.

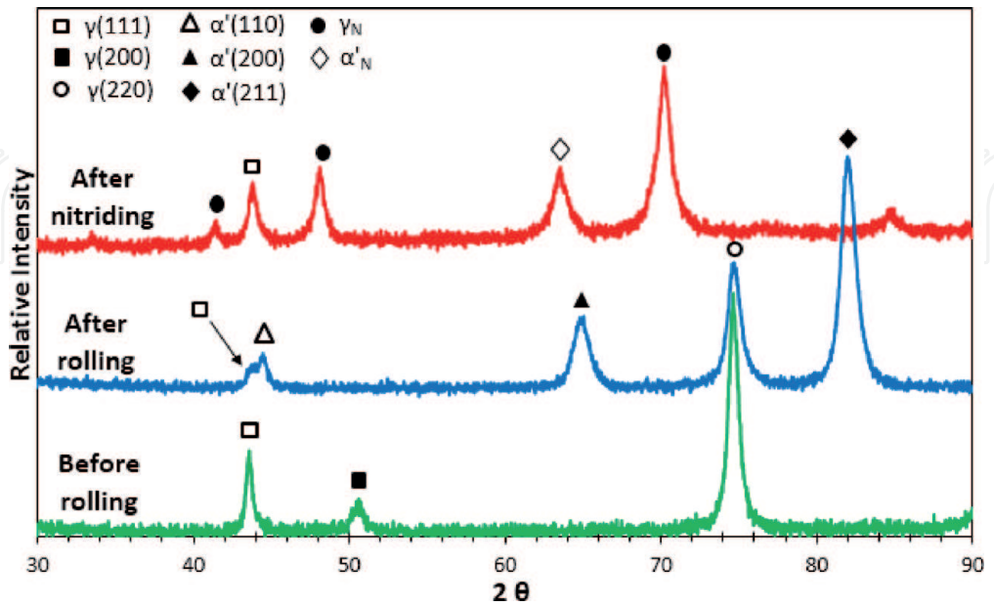


Figure 3.
Variation of XRD diagrams from the original AISI304 sheet before rolling to AISI304 after intense rolling and furthermore to rolled AISI304 sheet after low temperature plasma nitriding.

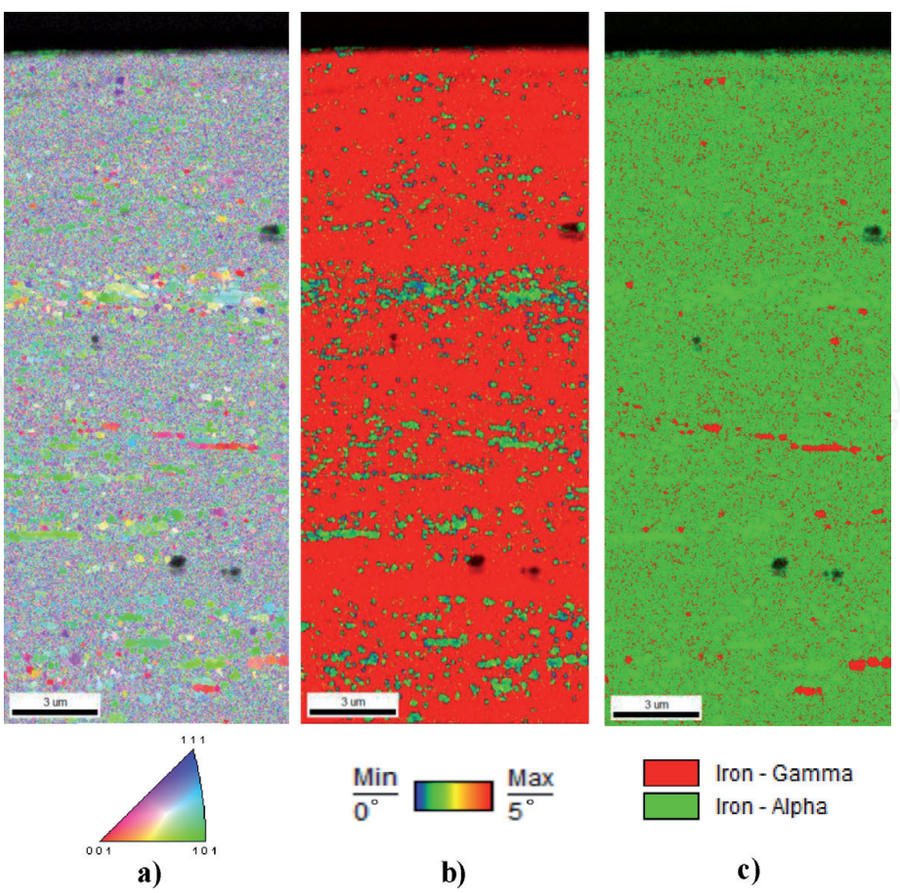


Figure 4.
EBSD analysis on the cross-section of rolled AISI304 sheet. (a) IPF mapping, (b) KAM distribution, and (c) phase mapping.

3. Crystallographic change by piercing

Fine piercing is an essential process in metal forming for accurate drilling of holes and for fine blanking. In the last decade, metastable austenitic stainless steel type AISI304 with fine grains has been developed by [18–20]; the effects of fine crystallographic structure on the elasto-plastic deformation have been closely studied in [21–23]. **Figure 5** shows three metastable austenitic stainless steel AISI304 sheets with the thickness of 100 μm, where the grain size was reduced by rolling process from the normal-grained sheet with the average grain size (D) of 7.5 μm. Two fine-grained AISI304 sheets were yielded to have D = 3.0 and 1.5 μm, respectively, by reverse transformation of the strain-induced martensitic phase. In this thermo-mechanical treatment, near-fully martensitic grains in **Figure 4c** are inversely transformed together with reduction of grain sizes [4, 7].

Their IPF maps analyzed by EBSD were shown on the cross section in the sheet width direction. When D = 7.5 μm, most of grains have a preferred orientation to [111] direction, as shown in **Figure 5a**. The crystallographic structure for D = 3 and 1.5 μm became nearly the same as D = 7.5 μm as depicted in **Figure 5b** and **c**.

3.1 Microstructure evolution by piercing

These AISI304 sheets with different grain sizes were pierced by CNC stamper under the same conditions; e.g., the punch diameter was 100 μm, the die diameter, 110 μm, and the clearance, 5% of sheet thickness. **Figure 6** compares IPF mapping as well as phase mapping on the cross-section of punched hole among three AISI304 sheets with the different grain size by D = 1.5, 3.0, and 7.5 μm. As commonly seen in **Figure 6a–c**, most of grains along the side surface of hole are distorted and refined in size. The shearing of AISI304 sheet by piercing leaves the process-affected zones along the shearing plane. The phase mapping in **Figure 5d–f** reveals that these process-affected zones are just corresponding to the martensitic phase [24]. That is, the original austenitic matrix to AISI304 sheets is forced to transform to martensite by the shearing strain during the piercing process. This strain-induced martensitic transformation is a non-diffusive shear transformation; each grain in the affected-process zone massively makes transformation [25, 26].

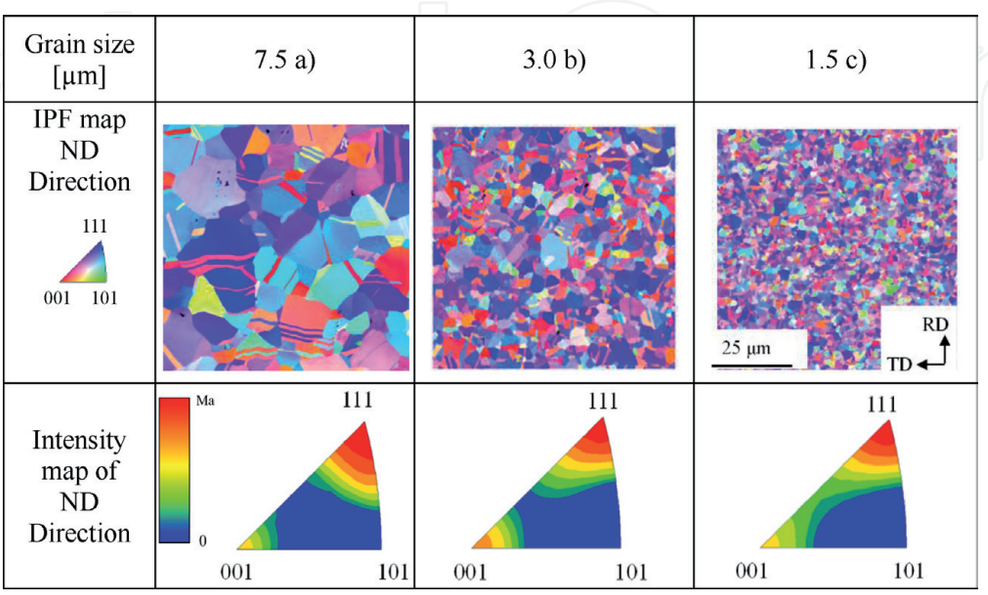


Figure 5.
IPF map and intensity map in the ND direction analyzed by EBSD. (a) Normal-grained AISI304 sheet with F = 7.5 μm, (b) fine-grained AISI304 sheet with D = 3.0 μm, and (c) fine-grained sheet with D = 1.5 μm.

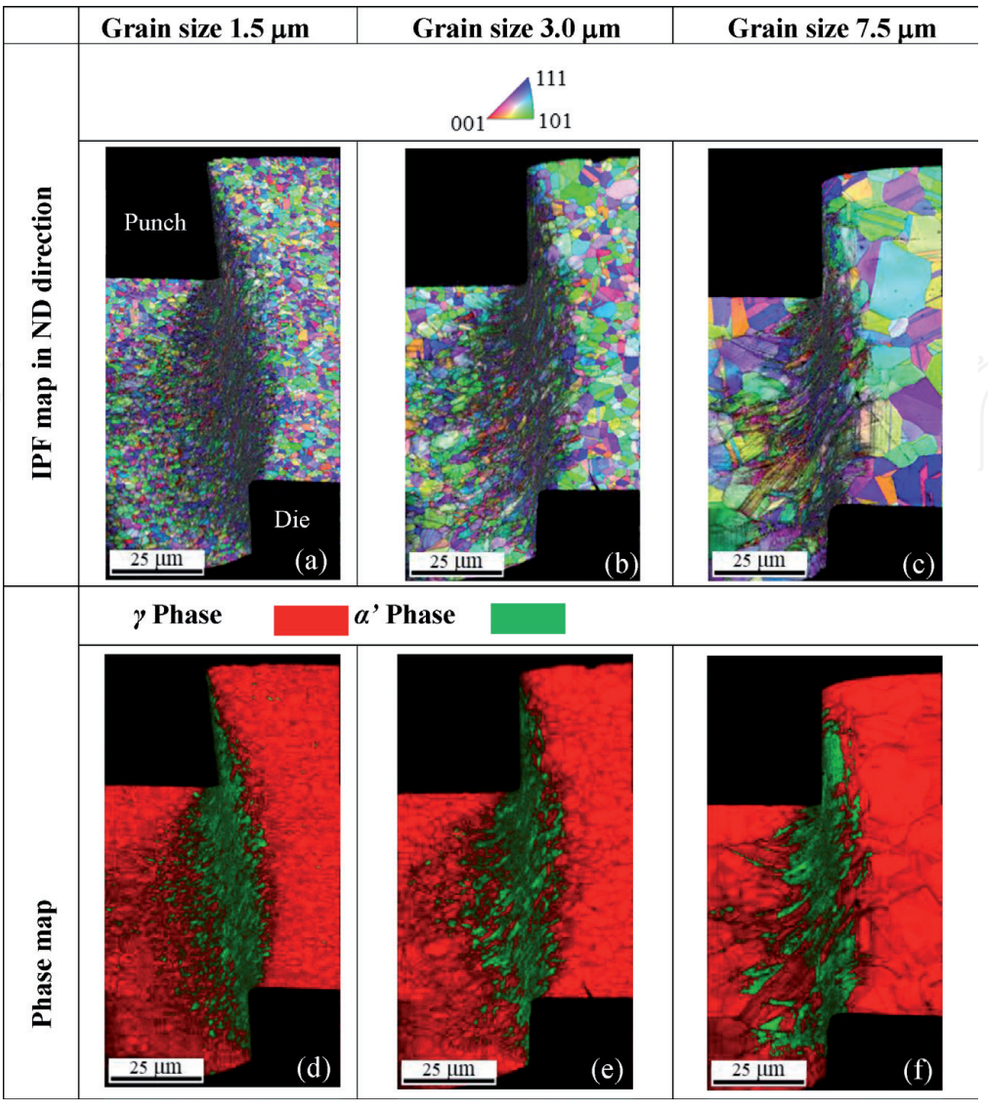


Figure 6.
EBSD analyses of IPF mapping in the ND direction and phase mapping on the cross-section of punched AISI304 sheet. (a) IPF map at D = 1.5 μm, (b) IPF map at D = 3 μm, (c) IPF map at D = 7.5 μm, (d) phase map at D = 1.5 μm, (e) phase map at D = 3 μm, and (f) phase map at D = 7.5 μm.

Let us consider the effect of average grain size on this formation of affected-process zones with phase transformation. When D = 7.5 μm, the zone boundary between the austenitic and martensitic phases is shaped to be irregularly jagged in **Figure 6d**. With decreasing the grain size, this phase boundary gradually is homogenized to be smooth as seen in **Figure 6e** and **f**. To be noticed, the volume of strain-induced martensitic phase in **Figure 6f** becomes larger than that in **Figure 6e**. This increase of strain-induced martensitic phase volume ratio causes the variation of the fracture length of the hole at the punch stroke direction [24].

3.2 Controlled crystallographic structure by piercing

The strain induced phase transformation in the process-affected zones by piercing is commonly observed in the metastable austenitic stainless steel sheets. Among them, the chemical components in each class of stainless steels have influence on the microstructure change by the piercing process. Two types of metastable austenitic stainless steel sheets were prepared as a work sheet with the thickness of 100 μm for piercing experiments under the same conditions as shown in **Figure 6**.

Figure 7 compares the phase mapping on the cross-section of punched holes between the stainless steel AISI316L and AISI304. When punching out the AISI316L sheet, the strain-induced martensitic phase hardly occurred along the shearing plane; no martensitic phase was present in **Figure 7a**. Instead of martensitic phase maps, the ferritic phase was strain-induced even by this piercing process as predicted by [27]. In fact, much ferrite was detected at the vicinity of die corner in **Figure 7a**. Let us consider why no martensitic phase but ferritic phase is induced by piercing the AISI316L sheet. As stated in [27], the nominal strain to induce the martensitic phase into AISI316L is two times larger than that to induce the ferrite phase. Hence, when piercing AISI3016L sheet, the ferritic phase is much easier to be induced than the martensitic phase. Therefore, even when the ferrite phase is induced along the shearing plane by the piercing process, each grain deformation is not hindered by shearing. As a result, the process-affected zone area in AISI316L becomes larger along the shearing plane in **Figure 7a** than that in AISI304 in **Figure 7b** [28].

The difference of crystallographic structure between pierced AISI304 and AISI316L sheets reveals that the process-affected zone formation could be controlled by the strain-induced phase transformation during the piercing process. EBSD analysis is really a well-defined means to describe the relationship between the strain-induced phase transformation by piercing and the crystallographic structure of pierced stainless steel sheets.

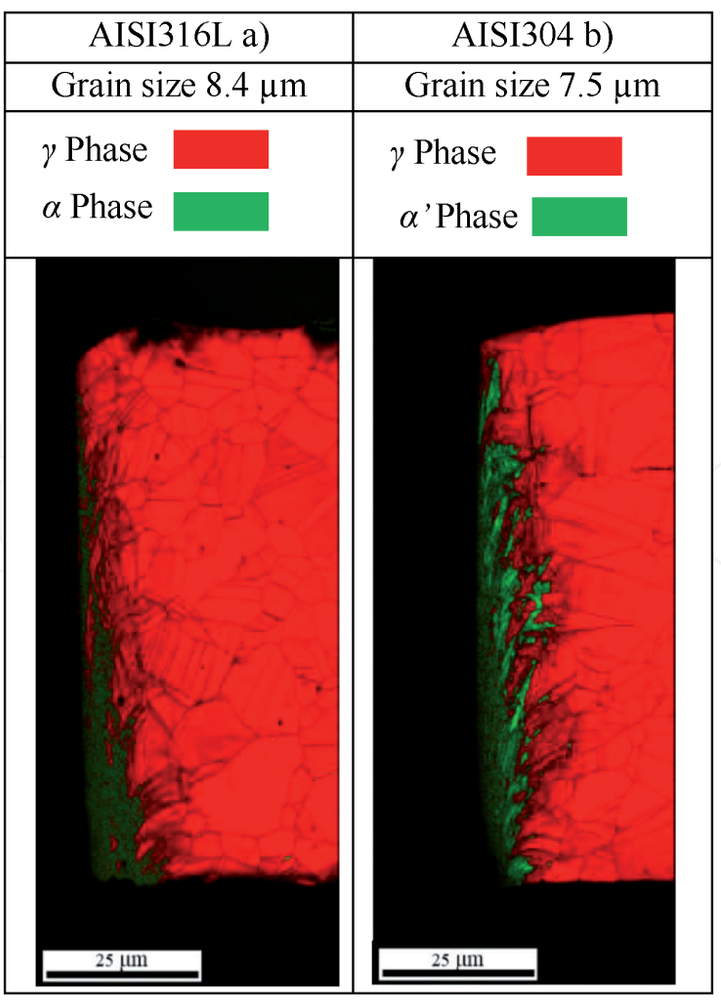


Figure 7.
Comparison of phase mapping on the cross-section of fully pierced AISI316L and AISI304 austenitic stainless steel sheets. (a) Punched-out AISI316L sheet and (b) punched-out AISI304 sheet.

4. Nanostructuring by low temperature plasma nitriding

Lower temperature plasma nitriding process of austenitic stainless steels than 700 K is governed by the nitrogen supersaturation with nitrogen interstitial occupation of octahedral vacancy sites of fcc-structured supercells as well as the nitrogen diffusion through refined grain boundaries and slipping lines [13–15]. FGSS316 plates and wires are employed to describe the nano-structuring process with grain size refinement by this plasma nitriding.

4.1 Low temperature plasma nitriding

High density RF (Radio Frequency) – DC (Direct Current) discharging plasma nitriding system is utilized to generate the nitrogen-hydrogen plasmas. **Figure 8** illustrates a typical hollow cathode device for homogeneously nitriding a single FGSS316 wire. RF-nitrogen/hydrogen plasma is ignited to surround the wire surface by a cylindrical plasma sheath. The activated nitrogen atoms (N^*) and ions (N^+) as well as the NH radicals are enriched in this sheath to increase the nitrogen ion density up to 1×10^{18} ions/m^3. Under this plasma processing condition, the nitrogen solute diffuses into the depth of FGSS316 matrix in wire to form the nitrided layer.

The inner nitriding process with nitrogen supersaturation is described by the multi-dimensional relation in **Figure 9**. When some nitrogen interstitial atoms diffuse and supersaturate the fcc-structured lattices in **Figure 9a**, their original lattice constant (Λ_0) increases to Λ by occupation of nitrogen interstitials into the octahedral vacancy sites in them. Other nitrogen atoms diffuse to further depth through the grain boundaries. Then, the nitrogen supersaturated (NS) zone expands with the elastic strain (ε_e) while unsaturated (US) zone does not deform; the strain incompatibility occurs on the boundary between NS and US zones. The misfit distortion (β_{misfit}) is induced along this zone boundary as depicted in **Figure 9b**; e.g., $\beta_{misfit} = \omega_{spin} + \varepsilon_p$, where ω_{spin} is a spin tensor to rotate the NS zone and to generate the crystallographic misorientation into a current zone, and ε_p, a plastic strain tensor to compensate for the strain incompatibility across the zone boundary. Nitrogen solutes further diffuse into the depth of grains through these zone boundaries, as shown in **Figure 9c**.

Through this multi-dimensional inner nitriding, high elastic strain energy density in NS zones drives the phase transformation from austenite to martensite. The spin rotation of zones and sub-grains advances with nitrogen diffusion and

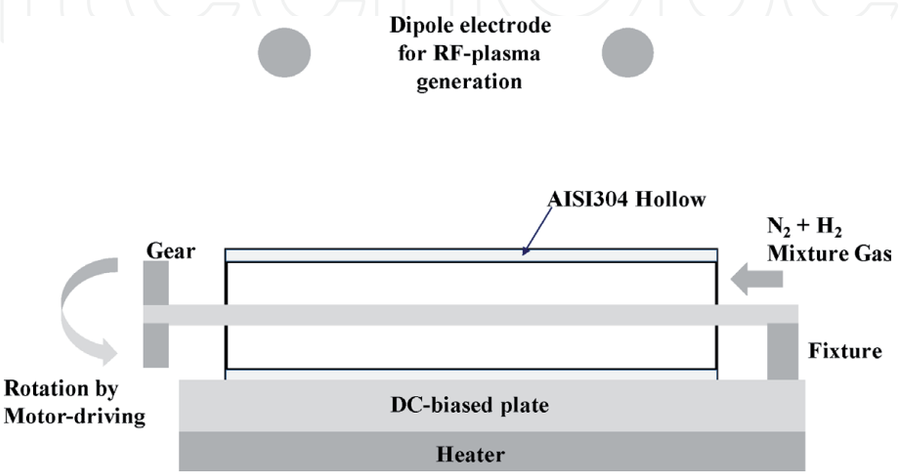


Figure 8.
Experimental setup for low temperature plasma nitriding of steel wires with use of the hollow cathode device. The same DC-bias was applied to the hollow and the FGSS316 wire.

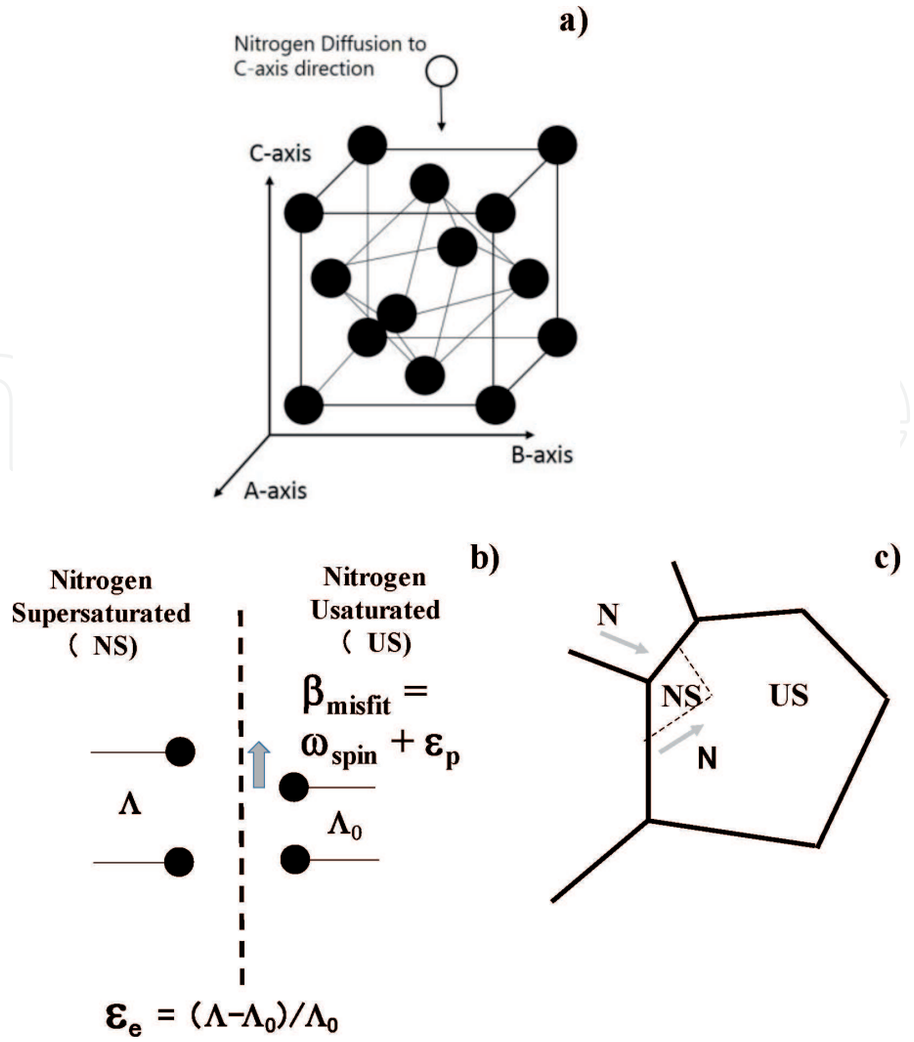


Figure 9.
Multi-dimensional relation in the nitrogen interstitial atom diffusion and supersaturation in the low temperature plasma nitriding.

supersaturation to refine the crystallographic structure. NS zones accompany with the plastic strain distribution along the NS-US zone boundaries.

This theoretical model is experimentally demonstrated in the following. As stated in [13–15], the inner nitriding advances homogeneously from the surface to the nitriding front end; it is rather difficult to experimentally describe each fundamental process separately from other processes in **Figure 9**. A normal-grained AISI316 plate is employed as a work material and nitrided at 623 K for 14.4 ks to decelerate the nitrogen diffusion rate and to describe the synergetic relation among the nitrogen supersaturation, the phase transformation, the plastic straining, the grain size refinement and the local nitrogen diffusion.

4.2 Microstructure evolution by inner nitriding in depth

Figure 10 depicts the homogeneous and heterogeneous inner nitriding processes in the nitrided AISI316 at 623 K for 14.4 ks. Under this nitriding condition, the high nitrogen solute content, [N], around 5 mass% is present down to the nitriding front end (NFE) at the depth of 30 μm. To be noted, [N] remains to be 1 mass % even below NFE, as shown in **Figure 10a**. This implies that homogeneous nitriding advances to NFE and changes to be heterogeneous by localization in nitrogen diffusion below NFE. In fact, the phase mapping as well as the crystallographic structure changes drastically across this NFE, which was indicated by the gray two-dots chain line in **Figure 10**.

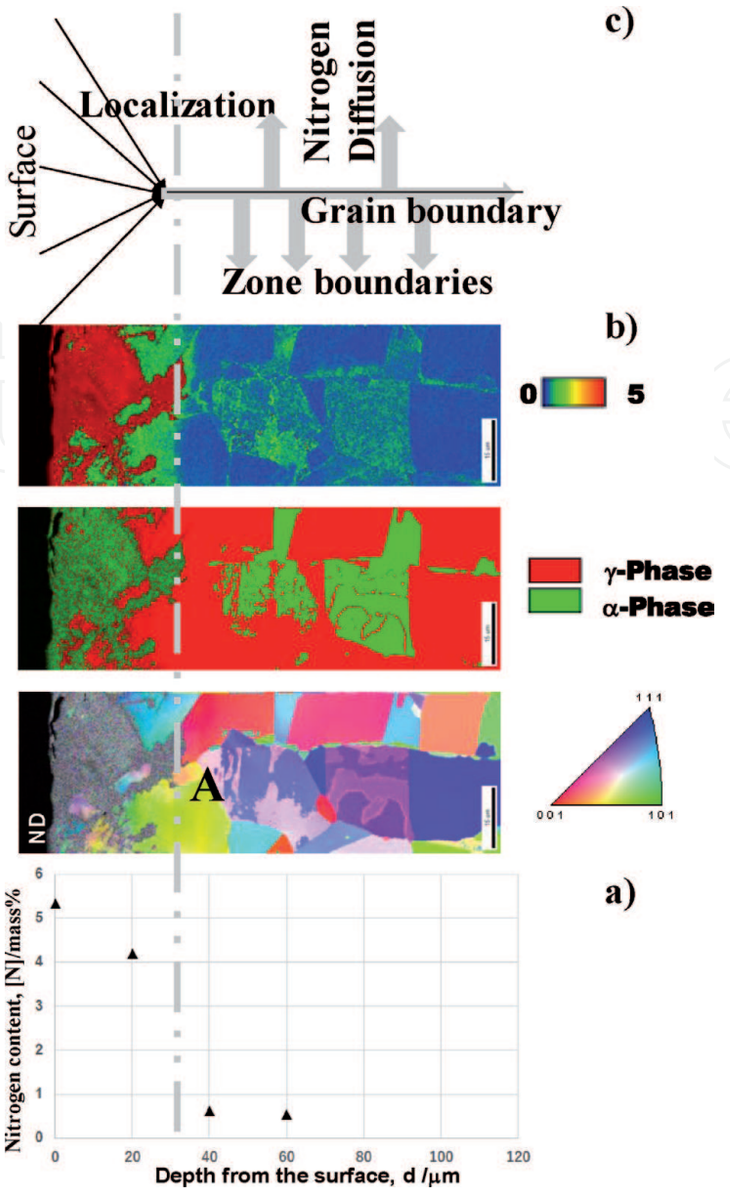


Figure 10.
Experimental demonstration on the inner nitriding process. (a) Nitrogen content depth profile, (b) IPF mapping, phase mapping and KAM distribution, and (c) inner nitriding mechanism.

Due to EBSD analysis, the synergetic relation is described by the inverse pole figure, the phase mapping and the plastic strain distribution below NFE in **Figure 10b**. The coarse grains near the grain boundary were only nitrided to change their microstructure; e.g., the austenitic and martensitic zones exclusively distribute in an A-grain. The retained austenitic zones in this grain had higher plastic strains (or higher KAM) and different crystallographic orientations from the martensitic zones, the plastic strains of which were much lower than these austenitic ones. This formation of γ- and α'-zone mixture with plastic straining and crystallographic rotation just corresponds to the multi-dimensional inner nitriding process. As depicted in **Figure 10c**, the nitrogen diffusion localizes across NFE so that the nitrogen selectively diffuses along the original grain boundary below NFE. This nitrogen main stream branches into the neighboring grains to this gran boundary. In each grain, the nitrogen further diffuses through the zone boundaries to drive the phase transformation, the plastic straining, and the refinement of zone sizes. Next, more precise EBSD analysis is made on this A-grain.

As compared between **Figure 11a** and **b**, little plastic strains were detected in the α'-zone of A-grain while the surrounding γ-zones were much plastically strained.

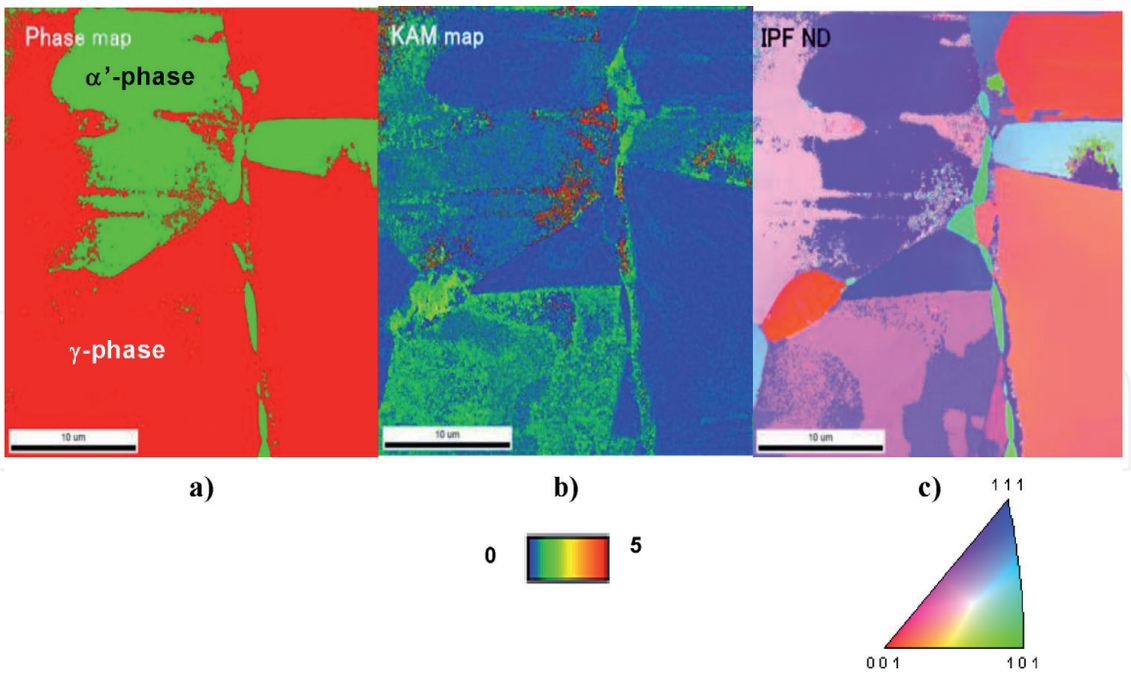


Figure 11.
Synergetic relation in the inner nitriding at 623 K, locally observed in the grain-A. (a) Phase mapping, (b) KAM distribution, and (c) IPF mapping.

This proves that some of NS-zones massively transform to α'-zones since the elastic strain energy density reaches to the critical level and that plastic strains are induced only in the neighboring γ-zones to α'-zones to compensate for misfit strain between NS-zones and surrounding unsaturated γ-zones. Comparing **Figure 11b** and **c**, these highly strained zones are just corresponding to crystallographically refined zones. This assures that spin rotations are induced together with the plastic strains by misfit distortion on the distributed zone boundaries to refine each zone size. Owing to this synergetic mechanism, the refined zones have mutual boundaries with high misorientation angles. This grain size refinement reflects on the high strength and hardness of the nitrided layer by the low temperature plasma nitriding.

4.3 Microstructure evolution in FGSS316 wires

As had been discussed in [29, 30], the initial grain size of AISI316 has influence on the inner nitriding behavior; homogeneity in nitriding process is enhanced with reduction of initial grain size. This finding suggested that fine-grained AISI316 or FGSS316 structural components and parts could be homogeneously nitrided on the surface with a little effect of heterogeneous nitriding on the microstructure below NFE. In the following, a FGSS316 wire is nitrided at 623 K for 14.4 ks and its microstructure is precisely analyzed to describe the formation of nitrided layer as well as the microstructure evolution at the surface and below NFE during this low temperature nitriding. **Figure 12** depicts the nitrogen solute mapping, phase mapping, and crystallographic structure on the lateral and longitudinal cross-sections of nitrided FGSS316 wire, respectively. The wire surface is surrounded by two-phase fine-grained layer with the thickness of 30 μm and the average nitrogen content of 5 mass% as seen in **Figure 12a** and **d**. The retained austenitic phase grains with larger size than nano-structured grains are present in the inside of nitrided layer as seen in **Figure 12b**, **c**, **e**, and **f**, respectively. This reveals that inner nitriding process advances almost homogeneously but that its synergetic relation is retarded in some parts to leave the nitrogen supersaturated γ-grains without phase

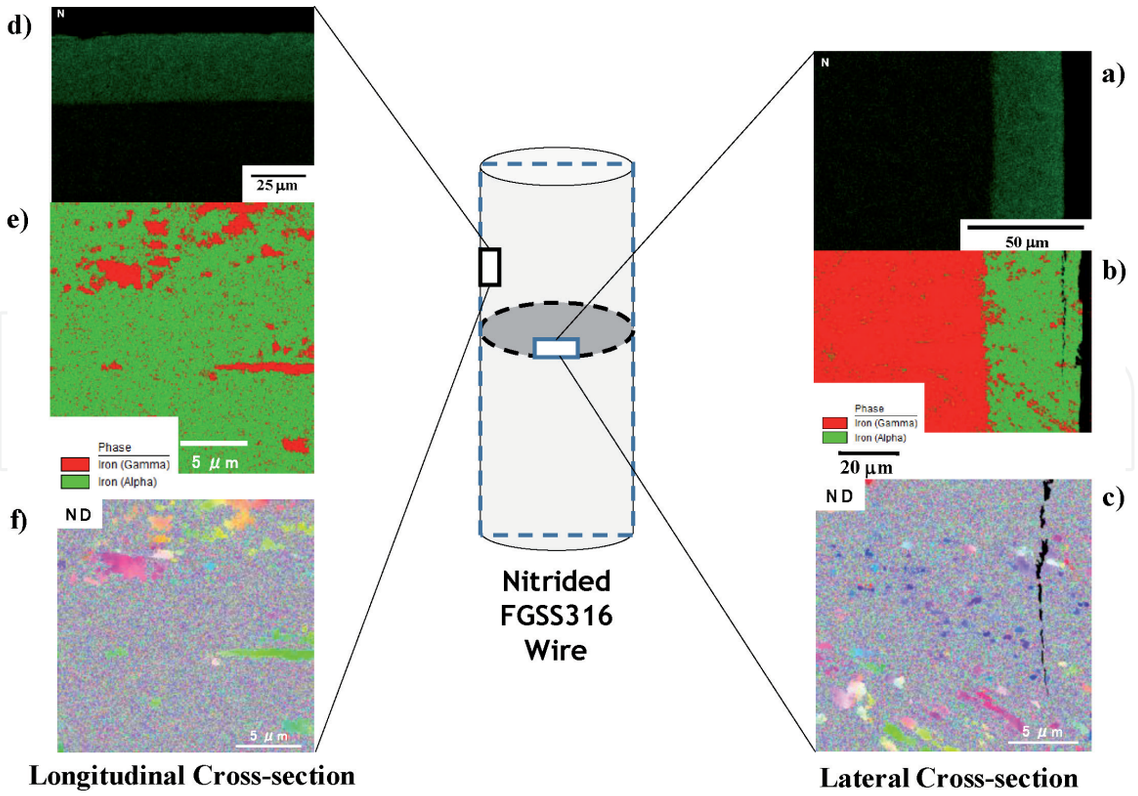


Figure 12.
Microstructure and nitrogen mapping across NFE on the lateral and longitudinal cross-sections of nitrided FGSS316 wire at 623 K for 14.4 ks. (a) Nitrogen mapping, (b) phase mapping, and (c) IPF mapping in the nitrided layer, on the lateral cross-section. (d) Nitrogen mapping (e) phase mapping in the nitrided layer, and (f) IPF mapping in the nitrided layer, on the longitudinal cross-section.

transformation and grain size refinement. In the following section, these retained γ-zones are employed as a marker to investigate the effect of uniaxial loading on the nitrided surface layer.

Let us analyze the effect of inner nitriding on the FGSS316 matrix below NFE. **Figure 13a** shows the initial microstructure of FGSS316 wire. This microstructure of FGSS316 before nitriding has equiaxial crystallographic structure with the average grain size of 2 µm. **Figure 13b** and **c** shows the crystallographic microstructure after nitriding on the lateral and longitudinal cross-sections of wire, respectively. The original microstructure is modified to form the skewed linear zones with finer grains as pointed by "b" in **Figure 13c**. These nitrogen-supersaturated zones consist of the transformed α'-zones and their surrounding plastic-strained. Just as discussed in **Figures 10** and **11**, the inner nitriding process advanced heterogeneously in the depth below NFE even when nitriding the FGSS316 wire.

4.4 Controlled crystallographic structure by plasma nitriding

Different from the metal forming, the plastic strains are induced along the network of subgrain and zone boundaries, which are newly generated in the inside of original matrix by nitrogen diffusion and supersaturation. Since this network also works as new nitrogen diffusion paths, further nitrogen diffusion and supersaturation advances into the depth of original grains. This concurrent co-working of nitrogen diffusion and supersaturation sustains the synergetic relation among the phase transformation, the plastic straining, and the grain size refinement. In particular, fine zone network results in refined nano-sized crystallographic structure after plasma nitriding.

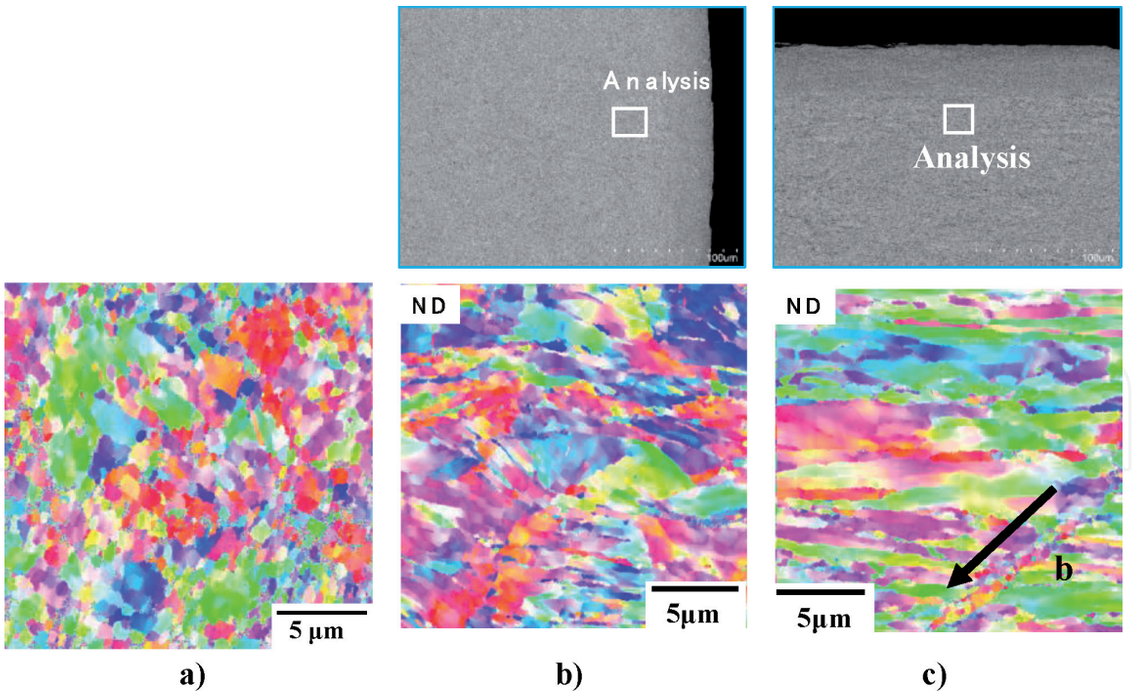


Figure 13.
Comparison of the crystallographic structure before and after plasma nitriding. (a) Initial microstructure of FGSS316 wire, (b) microstructure of FGSS316 matrix on its lateral cross-section, and (c) microstructure of FGSS316 matrix on its longitudinal cross-section.

5. Formation of bundle structures in nitrided wire by uniaxial loading

The nitrided FGSS316 wire is further uniaxially loaded in tensile. The austenitic grains are continuously linked between its nitrided layer and inner matrix. This nitrided layer had influence on the mechanical response of wire since the same elasto-plastic strains are applied to these two regions. Precise microstructure analysis is also made to describe the microstructure evolution of this nitrided wire during the uniaxial loading.

5.1 Uniaxial loading procedure

The uniaxial tensile loading test was performed by using the precision universal testing machine AUTOGRAPH AGS-X 10 kN (SHIMADZU Co. Ltd.). This uniaxial loading was terminated when the maximum applied load reached 6 kN before fatal ductile fracture for microstructure analyses. The applied load and stroke were in situ monitored by the load cell and linear scaler, respectively. The bare FGSS316 wire without nitrided layer has an ultimate strength (σ_U) of 1.18 GPa at the stroke (δ) of 4.9 mm, or, at the nominal strain (ε) of 0.17.

5.2 Microstructure evolution during uniaxial loading at RT

A normal FGSS316 wire elongates in the tensile direction at room temperature (RT) without significant change of microstructure except for the formation and coalescence of voids near the fatal ductile fracture of wire [31]. Microstructure of high carbon steel wire is sensitive to drawing process since it has a multi-dimensional microstructure, where each austenitic grain boundary houses pearlite blocks and each block consists of pearlite colony with the same lamellar structure of cementite (or θ-phase) and lamellar ferrite [32]. However, little microstructure

change occurs at the RT in its uniaxial tensile loading. A composite wire also has no microstructure evolution before pop-out of fibers from core matrix [33]. Let us investigate the microstructure at the nitrided layer and in the matrix of wire, respectively, and describe the effect of posterior elasto-plastic straining to nitriding on the microstructure evolution in wire.

Figure 14 depicts the plastic strain distribution and phase mapping on the lateral and longitudinal cross-sections of nitrided FGSS316 wire, respectively, after uniaxial loading. The retained austenite regions with larger size than fine grained two-phase nitrided layer in **Figure 12** completely disappear at the nitrided layer. Every nitrided layer has homogeneous two-phase microstructure with fine grain sizes. Compared with the plastic strain distribution before uniaxial loading, the whole nitrided layer is uniformly subjected to high plastic straining. This reveals that the applied plastic strains by uniaxial loading drives the synergetic process of inner nitriding at the retained austenitic zones and induces the phase transformation from the retained γ-phase to γ−/α'-phase fine mixture.

The microstructure as well as the phase in the matrix below NFE is modified by this uniaxial loading. Nearly full austenitic phase of matrix before loading changes to mixture of γ-fibers and transformed α'-fibers. As shown in **Figure 14b** and **d**, these α'-fibers with its lateral size of 0.5 μm are aligned along the loading direction to form a bundle structure together with γ-fibers. The volume fraction of these α'-bundles increases from the vicinity of NFE to the depth in matrix. This suggests that the nitrided FGSS316 wire fractures of α'-bundles in ductile at its center when this fraction reaches to the critical maximum.

Let us compare the above phase mapping in matrix with the plastic strain distribution in **Figure 14**. The high plastic straining zones are just corresponding to the α'-fiber zones. This proves that this γ to α'-phase transformation during the uniaxial loading is induced by the high plastic straining of γ-zones. That is, the highly strained γ-grains are plastically strained and aligned along the loading direction to form the γ-fibers. During this microstructure evolution, some of γ-fibers transforms massively to α'-fibers.

The phase transformation and formation of bundle microstructure in the above reflects on the crystallographic structure after uniaxial loading. **Figure 15** depicts the IPF mapping at the nitrided layer and in the matrix on the lateral and

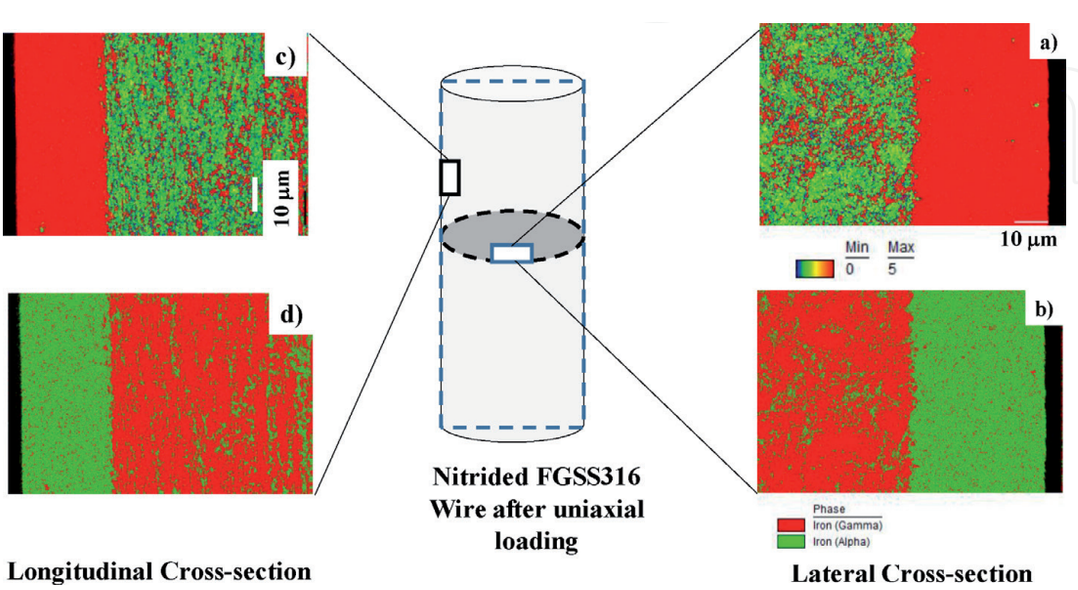


Figure 14.
Plastic straining and phase mapping on the lateral and longitudinal cross-sections of nitrided FGS316 wire after uniaxial loading. (a) Plastic strain lateral distribution, (b) phase mapping in lateral, (c) plastic strain longitudinal distribution, and (d) phase mapping in longitudinal.

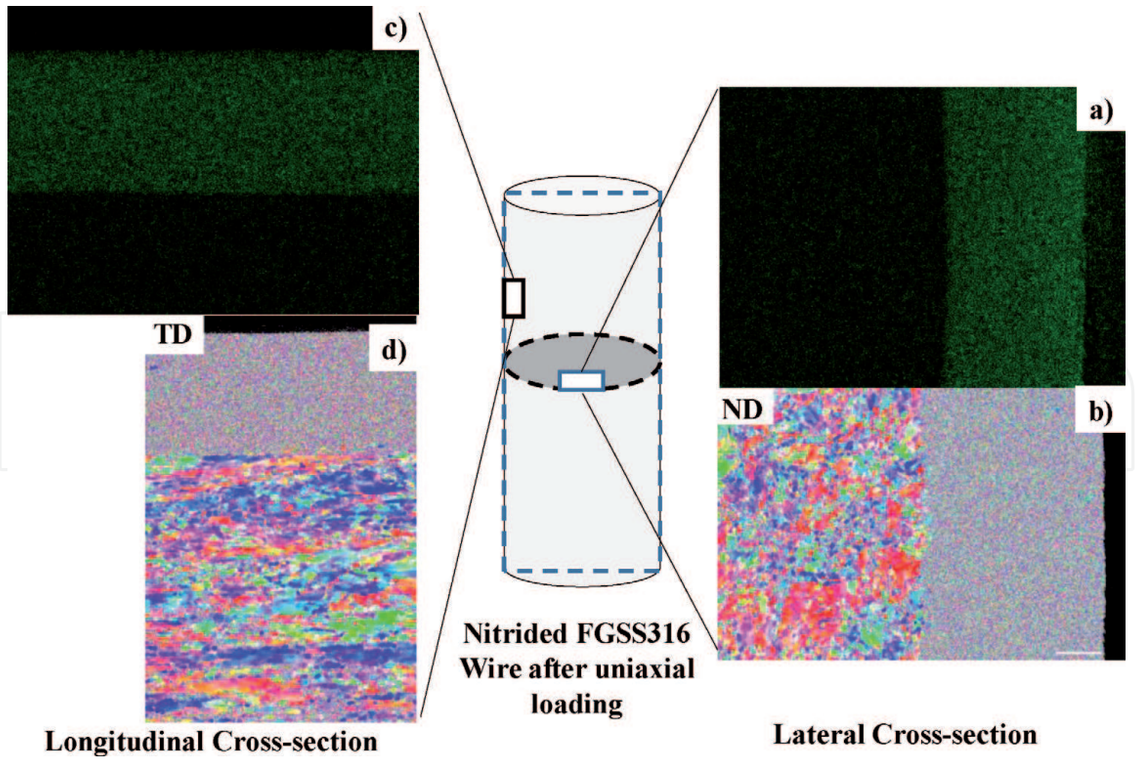


Figure 15.
Nitrogen mapping and crystallographic structure on the lateral and longitudinal cross-sections of nitrided FGSS316 wire after uniaxial loading. (a) Nitrogen mapping in lateral, (b) lateral IPF mapping in ND, (c) nitrogen mapping in longitudinal, and (d) longitudinal IPF mapping in TD.

longitudinal cross-sections of wire, respectively. The γ-phase matrix before uniaxial loading has crystallographic structure with the average grain size of 2 μm and without preferred orientations. After loading, these γ- and α'-grains are aligned along the loading direction respectively to form α'- and γ-bundles. In particular, most of α'-bundles have unique (111) directions. This might be because the transformed bundles are aligned in the tensile directions under the constrained conditions by the nitrided layer, surrounding the matrix. Each initial γ-grain is forced to deform elasto-plastically only in the tensile direction and to form γ-fibers and γ-bundles since no plastic deformation is allowed in the lateral direction under the confinement of nitrided layer. Some of strained γ-fibers makes massive transformation to α'-fibers; these α'-fibers are assembled into a single α'-bundle with the preferred orientation to (111). After [26, 34], the easiest crystallographic orientation to form this martensitic fibers and bundles is thought to be (111) tensile direction.

Figure 15 reveals that the nitrided layer surrounding the matrix has homogeneous super fine-grained two phase structure after uniaxial loading. No cracks and defects are seen on the nitrided layer surface and in the inside of layer; the fatal fracture of this nitrided FGSS316 wire occurs as the ductile fracture of matrix as explained before. The fine continuous interface between the nitrided layer and the matrix also suggests that elasto-plastic compatibility is preserved across this interface.

6. Discussion

The polycrystalline materials are generally described by the grain boundary characteristics and crystallographic orientation of each constituent grain as well as its grain size [35]. Each grain boundary energy is determined by the misfit orientation angle between adjacent grains. The compatible grain boundary has low energy enough to stack some amount of dislocations; while the incompatible one has high

energy enough to interact with dislocations [36]. In the metal forming of these polycrystalline materials or in the nitrogen supersaturation process, the dislocations as well as the slipping lines and planes interact with their grains and grain boundaries. In intense rolling, the grains are sheared and deformed to align their crystallographic orientation along the rolling direction and to form the textured microstructure. The applied elastoplastic distortion by rolling works to induce the phase transformation during rolling by high elastic strain energy density, to shear and elongate the grains by the plastic strains, and to spin the grain orientations toward the preferred one along the rolling direction. As reported in [37], the grain size is reduced down to sub-microns by repetitive rolling; due to small misorientation angles between adjacent grains, they are easy to agglomerate into larger grains by heat treatment.

In piercing, the grains near the shearing plane are affected by the applied elastoplastic distortion [38]. The increase of elastic strain energy density during piercing induces the phase transformation. The grains are sheared and fractured along the shearing plain. The original crystallographic structure of work materials is changed to align along the shearing plane by severe spinning with piercing. Although the grains are refined at the vicinity of shearing plain, the misorientation angles among them are small enough to be identified as nearly the same grain. Even in other metal forming processes than two in the above, their mechanical interactions of elastoplastic distortion with crystallographic structure is described by the strain-induced phase transformation, the shear deformation, the grain size refinement as well as the elastic recovery from the elasto-plastically strained state in unloading.

On the other hand, no elastoplastic distortion was directly applied to granular structure by the low temperature plasma nitriding. Instead of this direct straining, a large elastic distortion is induced into the nitrogen supersaturated zones in the work materials by lattice expansion. This distortion reaches to 10%, enough to drive the phase transformation in zones as well as the plastic distortion to compensate for the misfit on the zone boundaries between the nitrogen supersaturated and unsaturated ones. The symmetric component of this distortion works as a shearing strain tensor to form new slipping lines network across the original grain boundary. The asymmetric one drives spin-rotation in each zone to form the zone boundaries with high misorientation angles and to significantly refine the original grain size of work materials. Since those newly built-up zone boundaries play as a nitrogen diffusion path, this process advances concurrently with the nitrogen solute diffusion from the surface to the depth of materials. Since the zone size ranges in the nanometer order, the stainless steel work materials are covered by two-phase, nano-grained, nitrogen steel surface layer. The smallest zone size is determined by the mechanical balancing between the elastic straining in each material supercell and the slip-line formation surrounding it in the nitrogen supersaturation [39]. Precise TEM analyses down to the atomic scale are useful to describe the nitrogen interstitial atom distribution in the supercell [40].

Even when the rolled and pierced steel specimens are uniaxially loaded, their microstructure never changes themselves at room temperature before fracture. Their uniaxial stress-strain curves are determined by the original microstructure of as-rolled and as-pierced materials since no mechanical interaction occurs between the controlled grains by previous metal forming and the applied strain by uniaxial loading. On the other hand, the in situ microstructure evolution takes place during the uniaxial loading of the nitrided FGSS316 wire. The nitrogen supersaturated layer works a double role under this uniaxial tensile loading. The original FGSS316 matrix inside the wire is elastically supported by this nitrided layer. Since the austenitic grains are continuously linked with those in the nitrided layer, the matrix inside the wire is intensely elongated to change its microstructure to two-phase fibrous grains by the uniaxial loading. The microstructure in the as-nitrided layer is also affected by uniaxially applied plastic strains. The retained austenitic grains

with large size in the nitrided layer change themselves to two-phase, fine grains, which are the same as homogeneously nitrided nanostructure before uniaxial loading. This in situ refinement of granular structure in the nitrided layer reflects on the hardness profile. The original hardness of as-nitrided layer is 1400 HV; this is further enhanced up to 1600 HV after uniaxial loading. This proves that nitrogen could diffuse locally to the retained austenitic zones along the slip-lines by externally applied plastic straining and drive the nitrogen supersaturation process in them for refinement of their microstructure. Owing to the elastic constraint by the nitrided layer, the work-hardening process during the uniaxial loading is enhanced in the wire matrix to attain higher ultimate stress (σ_U); e.g., σ_U = 1.23 GPa in the nitrided FGSS316 wire at δ = 5.7 mm or at ε = 0.19.

This in situ microstructure evolution by uniaxial loading posterior to nitriding, suggests further possibility of crystallographic control to improve the mechanical properties of metallic works, takes place in the nitrided layer and in the matrix inside without mutual interactions. The microstructure evolution of low temperature nitrided members and parts in the above must be enhanced during warm and hot processing. After recent work on the high carbon steel wire during drawing [41, 42], significant reduction of lamellar ferrite distance as well as free carbon dissociation from the cementite lamellar structure in the perlite colony and block are responsible for high strengthening of high carbon steel wires. This implies that further carbon supersaturation is a key process to drive the in situ evolution to the preferred crystallographic microstructure to higher strength of wire. Owing to the equivalent role between carbon and nitrogen solutes to be working as an interstitial atom in steel [43], local nitrogen mobility from nitrogen supersaturated zone with high nitrogen content to NS-zones with lower nitrogen content could drive the in situ nitrogen alloying process of wire matrix during warm-/hot-drawing and rolling.

In this nitriding a priori to metal forming, FGSS316 wire was first nitrided and then uniaxially loaded. How about the plasma nitriding of the rolled AISI304 plate? As shown in **Figure 3**, the nearly full-martensitic phase of rolled AISI304 plate

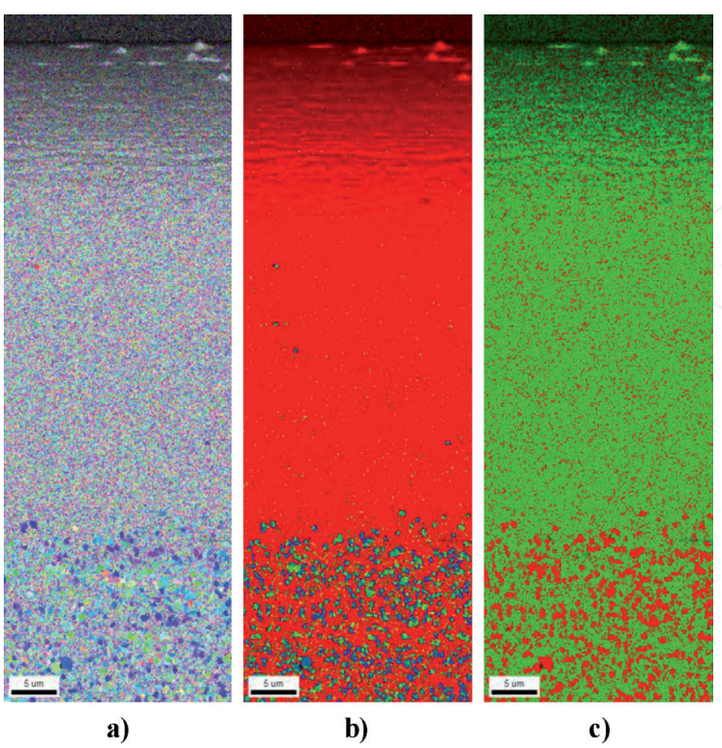


Figure 16.
Crystallographic structure on the cross-section of the rolled AISI304 plate after plasma nitriding at 673 K for 14.4 ks. (a) IPF mapping in the normal direction, (b) KAM distribution, and (c) phase mapping.

changed to a mixture of nitrided austenitic and martensitic phases. Since the original martensitic and austenitic peak positions shift to the low angle of 2θ and their peak widths become significantly broad, this mixture composes of the fine grained austenitic and martensitic zones with nitrogen supersaturation.

EBSD was also employed to describe this microstructure change of rolled AISI304 plate after nitriding. As shown in **Figure 16a**, the textured structure of rolled AISI304 completely disappeared and changed to fine-grained structure without preferred crystallographic orientation. This change is driven by high plastic straining in **Figure 16b**; every original grains with and without textures by rolling is plastically strained and spin-rotated by the nitrogen supersaturation to form homogeneous fine-grained structure. As depicted in **Figure 16c**, this fine microstructure consists of two phase with the fraction of martensite by 70%. This dramatic crystallographic structure evolution proves that posterior nitriding to metal forming is useful to further control the microstructure of stainless steels.

7. Conclusion

In the metal forming like intense rolling and fine piercing, the microstructure of work materials is changed by the applied plastic distortion with less influence to tool materials. In the rolling process, the original austenitic phase of stainless steels changes to be nearly full martensitic and to have textured microstructure with the preferred orientation to the rolling direction. This crystallographic structuring is intrinsic to the microstructure change by shearing with the reduction of thickness. In the piercing process by shear localization, the austenitic work material after piercing has new sheared and fractured surfaces including the affected zones. These zones consist of the phase-transformed martensite, the work-hardened austenite, and the elastically recovered zones. This crystallographic structure change is precisely described by EBSD on the cross-section of pierced work materials. In addition, various factors influence on this structure change including the grain size of work materials and the shear localization control as well as the chemical components in stainless steels.

In the low temperature plasma nitriding, no plastic strains are externally applied to work materials but nitrogen interstitial atoms are distributed from their surface to their depth with high concentration. Owing to the synergetic process in this inner nitriding process, the plastic distortion is concurrently induced by nitrogen diffusion and supersaturation. Since the nitrogen solute is homogeneously distributed in the nitrided layer with high content, the plastic distortion tensor also uniformly distributes in this layer. This homogeneous plastic distortion changes the normal crystallographic structure of AISI316 plates and wires; e.g., fine-grained AISI316 (FGSS316) microstructure of wires with the average grain size of 2 μm changes to the super-fine grained, two phase structure with the average grain size less than 0.1 μm. During this homogeneous nitriding, the retained austenitic zones distribute in the nitrided layer.

A priori nitriding to cold metal forming is a way to significantly control the microstructure and mechanical properties. The nitrided FGSS316 wire is elasto-plastically strained in the uniaxial direction so that the whole nitrided layers have fine-grained two-phase structure without retained austenite. This microstructure evaluation in local reflects on the homogeneous increase of hardness in the nitrided layer. This local interaction between nitrogen solute mobility and externally applied plastic strains at room temperature reveals that the microstructure and mechanical properties of nitrided work materials could be modified and improved by the metal forming posterior to the nitriding. In particular, the warm and hot post-treatment

by drawing, rolling, forging, and stamping has capability to control the crystallographic structure of nitrided parts and components.

Posterior nitriding to metal forming is another way to refine the microstructure and to improve the mechanical properties. In case when the rolled AISI304 plate is further nitrided at 673 K, its textured microstructure completely changes to super-fine grained, two phase structure. The intense plastic straining by nitrogen supersaturation also plays a role to control the crystallographic structure.

Acknowledgements

The authors would like to express their gratitude to Mr. T. Inohara (LPS-Works, Co., Ltd.), Mr. T. Yoshino, and Y. Suzuki (Komatsu-Seiki Kosakusho, Co., Ltd.) for their help in experiments. This study was financially supported by the METI-Program on the Supporting Industries at 2019.

Conflict of interest

The authors declare no conflict of interest.

Author details

Tatsuhiko Aizawa[1*], Tomomi Shiratori[2] and Takafumi Komatsu[3]

1 Surface Engineering Design Laboratory, SIT, Tokyo, Japan

2 University of Toyama, Toyama, Japan

3 Komatsu Seiki Kosakusho, Co., Ltd., Suwa, Nagano, Japan

*Address all correspondence to: taizawa@sic.shibaura-it.ac.jp

IntechOpen

© 2020 The Author(s). Licensee IntechOpen. This chapter is distributed under the terms of the Creative Commons Attribution License (http://creativecommons.org/licenses/by/3.0), which permits unrestricted use, distribution, and reproduction in any medium, provided the original work is properly cited. CC BY

References

[1] Callister WD Jr. Materials Science and Engineering. 7th ed. NJ, USA: John Wiley & Sons; 2007

[2] Friedel J. Les Dislocations. Paris, France: g-V; 1956

[3] Zhuang Z, Liu Z, Cui Y. Dislocation Mechanism-Based Crystal Plasticity. Beigin, China: Elsevier; 2019

[4] Tomimura K, Takaki S, Tokunaga Y. Reversion mechanism from deformation induced martensite to austenite in metastable austenitic stainless steels. ISIJ International. 1991;**31**(12):1431-1437

[5] Zhilyaev AP, Oh-Ishi K, Langdon TG, McNelley TR. Microstructural evolution in commercial purity aluminum during high-pressure torsion. Materials Science and Engineering: A. 2005;**410**:277-280

[6] Niue LL, Zhang Y, Shu X, Gao F, Jin S, Zhou H-B, et al. Shear-coupled grain boundary migration assisted by unusual atomic shuffling. Scientific Reports. 2016;**6**:23062

[7] Torizuka S, Umezawa O, Tsuzaki K, Nagai K. Shape, size and crystallographic orientation of the ferrite grains formed at grain boundaries of deformed austenite in a low carbon steel. Tetsu to Hagane. 2000;**86**(12):807-814

[8] Rosochowski A. Severe Plastic Deformation Technology. Scotland, UK: Whittles Publishing; 2013

[9] Aizawa T, Tokumitsu K. Bulk mechanical alloying for productive process of functional alloys. Materials Science Forum. 1999;**312**:13-22

[10] Aizawa T. Functionalization of stainless steels via low temperature plasma nitriding. In: Proceedings of the 7th Annual Basic Science International Conference. Malang, Indonesia; 2017. pp. 1-16

[11] Farghali A, Aizawa T. Phase transformation induced by high nitrogen content solid solution in the martensitic stainless steels. Materials Transactions. 2017;**58**:697-700

[12] Farghali A, Aizawa T. Nitrogen supersaturation process in the AISI420 martensitic stainless steels by low temperature plasma nitriding. ISIJ International. 2018;**58**(3):401-407

[13] Aizawa T. Low temperature plasma nitriding of austenitic stainless steels. In: Stainless Steels. London, UK: IntechOpen; 2018. pp. 31-50

[14] Aizawa T, Yoshihara S. Homogeneous and heterogeneous micro-structuring of austenitic stainless steels by the low temperature plasma nitriding. In: Proceedings of 7th International Conference on Material Strength and Applied Mechanics. Kita-Kyushu, Japan; 2018

[15] Aizawa T. Characteristics of nitrided layer in dies – Low temperature plasma nitrided stainless steels. Bulletin of the JSTP. 2019;**2**:411-415

[16] Chen Z, Yang Y, Jiao H. Some Applications of Electron Back Scattering Diffraction (EBSD) in Materials Research. London, UK: IntechOpen; 2012. DOI: 10.5772/3526

[17] Aizawa T, Shiratori T, Komatsu T. Integrated manufacturing of fine-grained stainless steels for industries and medicals. In: High Entropy Alloy. London, UK: IntechOpen; 2019. pp. 121-143

[18] Takagi S, Tanimoto S, Tomimura K, Tokunaga Y. Optimal chemical composition in Fe-Cr-Ni

alloys for ultra grain refining by reversion of deformation induced martensite. Tetsu to Hagane. 1988;**74**(6):1052-1057

[19] Tomimura K, Takagi S, Tokunaga Y. Reversion process of deformation induced martensite to austenite in metastable austenitic stainless steels. Tetsu to Hagane. 1988;**74**(8):1649-1655

[20] Katoh M, Torisaka Y. Thermo-mechanical treatment for improvement of superplasticity of SUS304. Tetsu to Hagane. 1998;**84**(2):127-130

[21] Torizuka S, Muramatsu E, Murty SN, Ngai K. Microstructure evolution and strength-reduction in area balance of ultrafine-grained steels processed by warm caliber rolling. Scripta Materialia. 2006;**55**(8):751-754

[22] Shiratori T, Suzuki Y, Nakano S, Katoh M, Yang M, Komatsu T. Influence of grain size on sheared surface in micropiercing. The Japan Society for Technology of Plasticity. 2015;**56**(652):401-406

[23] Shiratori T, Suzuki Y, Nakano S, Yang M, Komatsu T. Effects of grain size on the sheared surface in micropiercing of austenitic stainless steel SUS304. Manufacturing Review. 2015;**2**:9

[24] Shiratori T, Katoh M, Satoh N, Yoshino T, Nakano S, Yang M. Deformation and transformation behavior in micropiercing of fine-grained SUS304. The Japan Society for Technology of Plasticity. 2017;**58**(681):936-942

[25] Tamura I. On the TRIP steel. Tetsu to Hagane. 1970;**56**(3):429-445

[26] Shrinivas V, Varma SK, Murr LE. Deformation-induced martensitic characteristics in 304 and 316 stainless steels during room temperature rolling. Metallurgical and Materials Transactions A. 1995;**26A**:661-671

[27] Ameyama K. Low temperature recrystallization and formation of an ultra-fine (γ+α) microduplex structure in a SUS316L stainless steel. Scripta Materialia. 1998;**38**(3):517-522

[28] Shiratori T. Effects of grain size on strain induced martensitic phase after shearing deformation in micro punching at SUS316L steel. In: Proceedings of the 174th ISIJ Meeting. Vol. 30. Sapporo, Japan; 2017. p. 963

[29] Aizawa T, Yoshino T, Shiratori T, Yoshihara S-I. Grain size effect on the nitrogen super-saturation process into AISI316 at 623 K. ISIJ International. 2019;**59**:1886-1892

[30] Aizawa T, Shiratori T, Yoshino T, Suzuki Y, Komatsu T. Microstructure evolution of fine-grained AISI316 wire plasma nitrided at 623 K through uniaxial tensile loading. ISIJ International. 2020. (in press)

[31] Thomason PF. Ductile Fracture of Metals. Oxford, UK: Pergamon Press; 1990. p. 92

[32] Takahashi M, Nagumo M, Asano I. Microstructures dominating the ductility of eutectoid pearlitic steels. Journal of the Japan Institute of Metals. 1978;**42**(7):708-715

[33] Cuevas AC, Bercerril EB, Martinez MS, Riuz JL. Metal matric composites. Switzerland: Springer Nature; 2018. p. 221

[34] Tsurui T, Inoue S, Matsuda K, Ishigaki H, Murata K, Koterasawa K. Effect of tensile axis on α' martensitic formation of SUS304 stainless steel single crystals. Journal of the Society of Materials Science. 2001;**50**(10):1115

[35] Zakhariev Z, editor. Polycrystalline Materials. London, UK: IntechOpen; 2012

[36] Sutton AP, Balluffi RW. Overview on geometric criteria for low interfacial energy. Acta Metallurgica. 1987;**35**(9):2177-2201

[37] Ouchi C, Okita T. Austenitic grain refinement through static recrystallization immediately after hot rolling. Transactions of the Iron and Steel Institute of Japan. 1984;**24**:726-733

[38] Kalpakjian S, Schmid SR. Manufacturing Engineering and Technology. 5th ed. NJ, USA: Pearson Prentice Hall; 2006

[39] Aizawa T, Yohino T. Plastic straining for microstructure refinement in stainless steels by low temperature plasma nitriding. In: Proc. 12th SEATUC Conference. YagYagarta, Indonesia; 2018

[40] Wang ZW, Palmer RE. Atomic-scale structure analysis by advanced transmission electron microscopy. Frontiers of Nanoscience. 2015;**9**:127-159

[41] Tarui T, Yamasaki S. Microstructure and mechanical properties of high carbon steel wire. Bulletin of the JSTP. 2018;**1**(2):111-115

[42] Kajino S. Microstructure and mechanical properties of surface layer in drawn wire. Bulletin of the JSTP. 2018;**1**(2):116-120

[43] Domain C, Becquart CS, Foct J. Ab initio study of foreign interstitial atom (C, N) interactions with intrinsic point defects in α-Fe. Physical Review B. 2004;**69**:144122